



**HAL**  
open science

# Two-state model to describe the rheological behavior of vibrated granular matter

Ph. Marchal, C. Hanotin, L. Michot, S. Kiesgen de Richter

► **To cite this version:**

Ph. Marchal, C. Hanotin, L. Michot, S. Kiesgen de Richter. Two-state model to describe the rheological behavior of vibrated granular matter. *Physical Review E: Statistical, Nonlinear, and Soft Matter Physics*, 2013, 88 ((1)), pp.012201. 10.1103/PhysRevE.88.012207 . hal-00905705

**HAL Id: hal-00905705**

**<https://hal.science/hal-00905705>**

Submitted on 10 Mar 2022

**HAL** is a multi-disciplinary open access archive for the deposit and dissemination of scientific research documents, whether they are published or not. The documents may come from teaching and research institutions in France or abroad, or from public or private research centers.

L'archive ouverte pluridisciplinaire **HAL**, est destinée au dépôt et à la diffusion de documents scientifiques de niveau recherche, publiés ou non, émanant des établissements d'enseignement et de recherche français ou étrangers, des laboratoires publics ou privés.

**Two-state model to describe the rheological behavior of vibrated granular matter**Ph. Marchal,<sup>1,\*</sup> C. Hanotin,<sup>2</sup> L. J. Michot,<sup>3,†</sup> and S. Kiesgen de Richter<sup>2</sup><sup>1</sup>CNRS, Laboratoire Réactions et Génie des Procédés (LRGP-GEMICO), UMR 7274, Université de Lorraine, Nancy, F-54001, France<sup>2</sup>CNRS, Laboratoire d'Energétique et de Mécanique Théorique et Appliquée (LEMTA), UMR 7563, Université de Lorraine, Vandoeuvre-lès-Nancy, F-54504, France<sup>3</sup>CNRS, Laboratoire Interdisciplinaire des Environnements Continentaux (LIEC), UMR 7360, Université de Lorraine, Vandoeuvre-lès-Nancy, F-54501, France

(Received 27 February 2013; revised manuscript received 21 June 2013; published 25 July 2013)

In this paper, we present a model aimed at predicting the rheological response of a 3D dry granular system to nonstationary mechanical solicitations, subjected or not to vibrations. This model is based on a phenomenological two-state approach related to the inherent bimodal behavior of chain forces in granular packing. It is set up from a kinetic equation describing the dynamics of the contact network. To allow experimental assessment, the kinetic equation is transformed into a differential constitutive equation, relating stress to strain, from which rheological properties can be derived. Its integration allows predicting and describing several rheological behaviors, in stationary and nonstationary conditions, including viscous (Newtonian) and frictional (Coulombian) regimes, as well as elastic linear (Hookean and Maxwellian) and nonlinear behaviors. Despite its simplicity, since it involves only three independent parameters, the model is in very close agreement with experiments. Moreover, within experimental errors, the values of these parameters are independent of the type of test used to determine them, evidence of the self-consistency of the model.

DOI: [10.1103/PhysRevE.88.012207](https://doi.org/10.1103/PhysRevE.88.012207)

PACS number(s): 83.80.Fg, 47.57.Gc, 47.57.Qk

**I. INTRODUCTION**

Understanding granular packing stability is of major importance in numerous natural and industrial situations. For instance, packing stability plays a crucial role in the triggering of avalanches or landslides or in the blocking of industrial silos. Despite intrinsic differences linked to the non-Brownian nature of granular materials, their rheological behavior is by many aspects rather similar to that of complex colloidal media (polymers, surfactants, dispersions...). In particular, granular media behave either as solids or liquids, depending on the mechanical solicitations to which they are subjected. Still, recently developed mesoscopic models, such as SGR, STZ, or MCT [1–4], that capture some of the flow and deformation features of amorphous materials are not able to account for all experimentally observed rheological behaviors of flowing granular matter [5–8]. This is certainly linked to the discrete, macroscopic nature of granular materials. Indeed, in response to some change in external forces, the macroscopic behavior of a granular system is related to the evolving structure of its contact network [9–11] and to the nature of the contacts themselves (frictional interactions, sliding or not) [12,13].

Recent experimental [14,15] and simulation [13,16] works have shown that it was relevant to describe 3D granular packings as the combination of two contact networks, a weak one and a strong one, that evolve independently from each other in response to external solicitations. Strong contacts ensure cohesion, momentum transport, and linear elastic properties, whereas weak contacts dominate nonlinear effects. Therefore, the way stress propagates through the network

of intergranular contacts strongly depends on sample density and on the spatial configuration adopted by the grains, after sample conditioning inside characterization devices [17–19]. As a consequence, to perform representative measurements that are not sensitive to the particular topology of a stack, it is crucial to obtain information that is averaged over all the accessible configurations. Unfortunately, granular media being macroscopic athermal systems, their initial configurations do not evolve spontaneously. A way to overcome this problem could be to use vibrations. Indeed, it has recently been shown that vibrations (even of small amplitude) influence the rheology and the dynamics of grains in granular packings [20–32]. Furthermore, D'Anna *et al.* [26,27,33–35] have discovered that the motion of a torsion oscillator immersed in an externally vibrated granular medium of glass spheres is Brownian-like. In the case of granular materials, using mechanical energy is analogous to the use of thermal energy for Brownian systems.

In that context, we have developed a powder rheometer prototype equipped with a vibrating cell [23,24,36]. Using such a setup, we have been able to carry out detailed studies of the rheological features of vibrated powders under stationary solicitations [20–24]. At low stationary stress, the viscosity exhibits a Newtonian behavior controlled by the energy injected by vibrations, whereas the behavior remains frictional and independent of vibrations at higher stress. It has further been shown in Marchal *et al.* [23,24] that the Newtonian behavior could be predicted on the basis of a rheological model assuming a Maxwell-Boltzmann distribution of free volumes in vibrated granular matter [37–40]. In the present paper, we develop a simple phenomenological model, based on the dynamics of the contact network, to predict the rheological response of a 3D vibrated dry granular packing subjected to nonstationary solicitations, thus extending our previous analyses. We show that a simple two-state model related to the inherent bimodal behavior of chain forces in

\*philippe.marchal@univ-lorraine.fr

†Present address: CNRS, Physicochimie des Electrolytes, Colloïdes et Sciences Analytiques (PECSA), UMR 7195, Université Pierre et Marie Curie, Paris Cedex 5, F-75222, France.

granular packing associated with a detailed balanced equation describing transition rules between these two states can predict, in part, the rheological behavior of vibrated and sheared granular matter in both stationary and nonstationary conditions.

**II. MODEL**

**A. A toy experiment: the “stick stuck” effect**

A well-known simple experiment, the “stick stuck” experiment [41], will serve as a starting point for modeling (Fig. 1). In this experiment, a wooden stick is introduced [Fig. 1(a)] in a container filled with compacted granular medium (such as sand or powdered sugar). After a slight compaction of the sample, the stick is pulled vertically so that the grains tend to move slightly with respect to each other. Under the principle of Reynolds dilatancy [42,43], a compacted granular medium can only be deformed by increasing its volume: grains must move away from each other to exit from the interstices formed by their nearest neighbors. In a medium confined by rigid walls, dilatancy results in a compression of the grains against each other, leading to the formation of arches between the stick and the container [Fig. 1(b)]. Therefore, a consolidation stress is induced between the grains up to a value related to the weight of the sample. If the stress exerted via the stick is higher than the consolidation stress, a critical deformation  $\gamma_c$  is exceeded, resulting in a rupture of the arches and the drop of the container [Figs. 1(c) and 1(d)]. Conversely, as long as this stress does not exceed the consolidation stress, the arches are strong enough to allow the rising of the container and its contents upon the rise of the stick [Fig. 1(e)]. However, when the system is subjected to slight vibrations, a liquefaction phenomenon occurs, arches are destabilized, and the container falls [Figs. 1(f) and 1(g)]. This experiment shows that the grains form a contact network consolidated by shear in the limit

of small deformations ( $\gamma < \gamma_c$ ) but destabilized by the same shear at large strains ( $\gamma > \gamma_c$ ). Vibrations clearly destabilize the network through a liquefaction process, since it is impossible to lift the container with the stick when the sample is subjected to vibrations. This experiment shows that in a vibrated granular medium under shear, at a given time  $t$ , some grains are in contact and are able to ensure stress transmission while others are disconnected and unable to provide such a transmission. It then appears that a given grain can only be in two distinct states: a consolidated state ( $C$ ) that ensures momentum transport and a mobile state ( $M$ ) disconnected. The granular medium, thus, reduces to a two-level system [44], the transition between these states being ensured by vibrations and shear.

**B. A two-state model for vibrated granular matter**

Since only the grains in the state ( $C$ ) ensure momentum transport, we use as a variable of state the fraction of grains  $P_C = N_C/N_p$ , where  $N_C$  is the number of grains in the state ( $C$ ) and  $N_p$  the total number of grains. In other words,  $P_C$  is the occupation probability of state ( $C$ ) as  $P_M + P_C = 1$ , where  $P_M$  is the occupation probability of state ( $M$ ) (Fig. 2).

The temporal evolution  $\dot{P}_C(t) = \frac{dP_C(t)}{dt}$  of the fraction of grains in the state ( $C$ ) is equal to the fraction of grains evolving from ( $M$ ) to ( $C$ ) minus the fraction of grains making the reverse transition per unit of time:

$$\begin{aligned} \dot{P}_C(t) &= \omega_{CM}(t)P_M(t) - \omega_{MC}(t)P_C(t) \\ &= \omega_{CM}(t)[1 - P_C(t)] - \omega_{MC}(t)P_C(t). \end{aligned} \quad (1)$$

Equation (1) is a balance equation related to the average probability  $P_M$  and  $P_C$  of occupation of states ( $M$ ) and ( $C$ ). Consequently, the kinetic constants  $\omega_{CM}$  and  $\omega_{MC}$  are the frequencies or probabilities of transition per unit time between states ( $M$ ) and ( $C$ ).

The “stick stuck” experiment shows that on average  $C \rightarrow M$  transitions, which correspond to the rupture of the contacts network, are induced by both shear and vibrations. On the one hand, the probability of transition induced by vibrations is, by definition, equal to the Brownian reorganization frequency  $f_b$  of the grains [23,24]. On the other hand, the probability of reorganization induced by shear is equal to the frequency at which the grains are disconnected when the critical strain  $\gamma_c$  is exceeded. It is then proportional to shear rate  $\dot{\gamma}$ . As these two processes are uncorrelated, the total transition frequency  $\omega_{MC}$

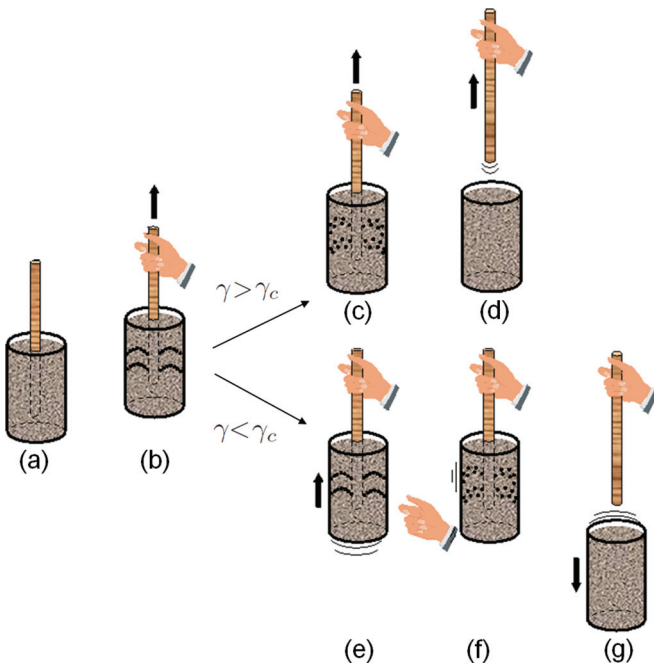


FIG. 1. (Color online) The “stick stuck” experiment.

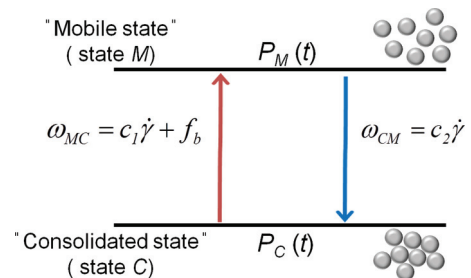


FIG. 2. (Color online) The two-state model used to describe the rheological behavior of granular matter subjected to vibrations and shear.  $P_C(t)$  and  $P_M(t)$  are, respectively, the probability of occupation of state ( $C$ ) and ( $M$ ) at time  $t$ .

is simply equal to the sum of the frequencies of reorganization corresponding to each process (*addition law*). In contrast,  $M \rightarrow C$  transitions are only due to shear. Therefore, the frequency  $\omega_{CM}$  at which the grains are put in contact with each other is also proportional to  $\dot{\gamma}$ . It follows that

$$\omega_{MC} = c_1\dot{\gamma} + f_b \text{ and } \omega_{CM} = c_2\dot{\gamma}. \quad (2)$$

With  $\gamma_c = 1/(c_1 + c_2)$ , Eq. (1) can be written

$$\begin{aligned} \dot{P}_C(t) &= c_2\dot{\gamma}(t)[1 - P_C(t)] - [c_1\dot{\gamma}(t) + f_b]P_C(t) \\ \iff \dot{P}_C(t) + \left[ \frac{\dot{\gamma}(t)}{\gamma_c} + f_b \right] P_C(t) &= c_2\dot{\gamma}(t). \end{aligned} \quad (3)$$

In practice, the structural variable  $P_C$  is not experimentally measurable. It is then necessary to relate it to an observable rheological variable for transforming kinetic Eq. (3) into a rheological equation accessible to experiment. If one considers the stress as a diffusive flux of momentum and by assuming that it is transported by channels constituted by the “strong contacts network,” it appears that the number of channels increases with the number of consolidated grains. According to such a hypothesis, a heuristic way to turn Eq. (3) into a constitutive rheological equation is to assume that the stress is proportional to the fraction of grains in state ( $C$ ). The consequence of such a choice will be tested, *a posteriori*, against experiments in the following. Indeed, writing  $\sigma(t) = aP_C(t)$  in Eq. (3) leads to

$$\begin{aligned} \dot{\sigma}(t) + \left[ \frac{\dot{\gamma}(t)}{\gamma_c} + f_b \right] \sigma(t) \\ = G\dot{\gamma}(t) \iff \dot{\gamma}(t) = \gamma_c \frac{\dot{\sigma}(t) + f_b\sigma(t)}{G\gamma_c - \sigma(t)}. \end{aligned} \quad (4)$$

Where  $G = ac_2 = \text{cte}$  ( $\forall \dot{\gamma}$ ).

The evolution of a macroscopic system, induced by a random process [45], can be modeled by a kinetic equation like Eq. (3) if the system loses the memory of its previous microscopic states. Such memory loss must occur over a period much shorter than the macroscopic characteristic time of its macroscopic evolution [46]. At the microscopic scale, the transitions between different states of the system are due to the formation and breaking of intergranular contacts. The characteristic time corresponding to such a phenomenon refers to the duration of rearrangements between grains. The dimensional analysis of dense granular flows has revealed that, at the microscopic scale, the only relevant microscopic time for rigid grains of diameter  $d_p$  and density  $\rho_p$  is the confinement time  $t_{cf} = d_p\sqrt{\rho_p/P}$  [6,7]. It corresponds to the time a destabilized particle takes to fall into a neighboring gap of size  $d_p$  under the confining pressure  $P = \phi\rho_p gz$ , corresponding to the normal stress exerted on the grains,  $\rho = \phi\rho_p$  being the mass density of a sample of volume fraction  $\phi$  and  $z$  the depth at which the grain is located within the sample. For glass beads of diameter  $500 \mu\text{m}$  at a volume fraction  $\phi$  of 0.6, considering  $\rho_p \approx 2500 \text{ kg m}^{-3}$ ,  $z \approx 10^{-2} \text{ m}$ , and  $P \approx 150 \text{ Pa}$ , one obtains  $t_{cf} \approx 2 \times 10^{-3} \text{ s}$ . It must be pointed out that, at the microscopic scale, the Hertzian contact time  $t_{hz}$  should also be considered. This time is related to the time  $t_{el}$  corresponding to the dissipation of the mechanical energy via elastic waves propagation through the material. For instance, for glass beads

such as  $G \approx 7 \times 10^{10} \text{ Pa}$ , one obtains [47]:  $t_{hz} = (\frac{d_p^2 \rho_p}{G \dot{\gamma}^{1/2}})^{2/5} \approx 2 \times 10^{-6} \text{ s}$  for  $\dot{\gamma} = 1 \text{ s}^{-1}$ .  $t_{hz}$  being approximately three orders of magnitude lower than  $t_{cf}$ , analyzing the systems over time periods that are large with regard to  $t_{cf}$ , ensures a proper separation of time scales. In such conditions, granular reorganization can likely be described using a Markovian approach and should, therefore, be reasonably described using a kinetic equation such as Eq. (3). We will in the following test such an assumption by comparing experimental rheological measurements with predictions derived from Eq. (4). We focus in the present case on the response of the vibrated samples to *nonstationary solicitations*, i.e., stress steps or sinusoidal stresses. This significantly extends the analysis carried out in Ref. [24] that was restricted to stationary situations only.

### III. EXPERIMENTAL RESULTS

#### A. Material and methods

Glass beads samples (Total mass  $m = 130 \text{ g}$ , mean diameter  $530 \mu\text{m}$  with a standard deviation of  $90 \mu\text{m}$ ) were analyzed by both creep tests (steps of stresses) and mechanical spectroscopy (sinusoidal stresses). All experiments were carried out using a stress-imposed rheometer (AR2000, TA Instruments) equipped with a “powder cell,” able to generate granular reorganizations into the powder. This cell includes a four blades vane device plunging into a baffled cylindrical cup, which prevents sample slipping. The device is connected to a vibration exciter (Mini-shaker, Bruel and Kjaer) controlled by a function generator and an accelerometer (Fig. 3). Vibrations are sinusoidal and the energy  $E_v$  supplied to the granular medium is  $E_v = m(2\pi f)^2 A^2/2$ , where  $m$  is the sample mass and  $f$  and  $A$ , the frequency and amplitude of the vibrations.  $E_v/m$  is a key factor that has been shown to control the dynamics of the intergranular contact network [24]. It is proportional to the energy injected among the grains and it can be assimilated to a granular temperature since it follows similar laws as true temperature associated with Boltzmann’s statistics. Accordingly,  $f_b$  is an increasing function of  $E_v$  as shown in Ref. [24] and in Appendix A, in the same way as Brownian collision frequency between microscopic particles is an increasing function of  $kT$  in molecular or colloidal systems.

Creep tests were carried out for various stresses and for different values of the vibration energy  $E_v$ . Mechanical spectroscopy experiments were also carried out for different vibration energies, but in the following, for concision reasons, we will only show results obtained for a given frequency and energy ( $f = 50 \text{ Hz}$ ,  $A = 0.16 \text{ mm}$ ,  $E_v = 164 \mu\text{J}$ ). So, we focus here on the transient regime via creep tests and mechanical spectroscopy at a given frequency ( $f = 50 \text{ Hz}$ ,  $A = 0.16 \text{ mm}$ ,  $E_v = 164 \mu\text{J}$ ). The experimental results obtained for different values of the vibration energy are summarized in Appendix A.

Prior to each rheological test, the samples were submitted to vibrations over periods long enough to ensure stationary states of compaction. Rheological parameters ( $\sigma$ ,  $\gamma$ ,  $\dot{\gamma}$ ) are obtained from the evolution of torque ( $C$ ) versus angular rate ( $\dot{\theta}$ ) data via a calibration procedure leading to the determination of two

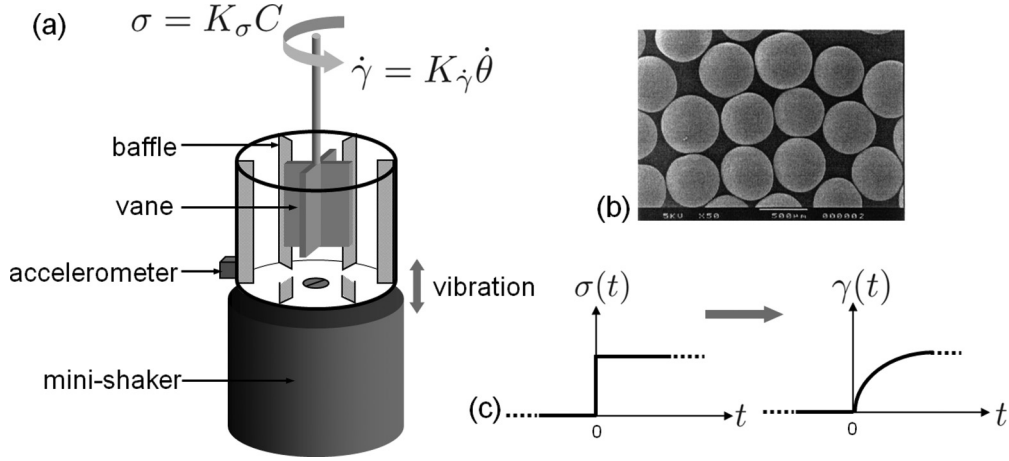


FIG. 3. (a) Experimental setup. (b) Microscopic snapshot of glass beads of the sample. (c) Measurements principle.

geometrical factors  $K_\sigma$  and  $K_\dot{\gamma}$ , such as  $\sigma = K_\sigma C$  and  $\dot{\gamma} = K_\dot{\gamma} \theta$ . Considering the measuring cell as a Couette device,  $K_\sigma$  and  $K_\dot{\gamma}$  are determined by solving the equation of motion with boundary conditions imposed by the geometrical dimensions of the inner and outer cylinders, in the case of a generalized Newtonian fluid obeying a power law model. Such a choice is not restrictive since any generalized Newtonian fluid can be asymptotically assimilated to a power law fluid. A more detailed description of the equipment and of the calibration procedure can be found in Ref. [24].

## B. Rheological behavior of the samples

### 1. Response to a stress step

In the case of a stress step defined as  $\sigma(t) = 0$  for  $t < 0$  and  $\sigma(t) = \sigma$  for  $t > 0$  [Fig. 3(c)], the integration of Eq. (4) yields (Appendix B)

$$\begin{aligned} \gamma(t) &= \gamma_c \frac{f_b t}{\frac{G\gamma_c}{\sigma} - 1} - \gamma_c \ln \frac{1}{\gamma_c} \left( \frac{G\gamma_c}{\sigma} - 1 \right) + \gamma_c \ln \left( \frac{G}{\sigma} \right) \\ &= \gamma_c \left[ \frac{f_b t}{\frac{G\gamma_c}{\sigma} - 1} - \ln \left( 1 - \frac{\sigma}{G\gamma_c} \right) \right]. \end{aligned} \quad (5)$$

Differentiating Eq. (5), one obtains the expression of the shear rate  $\dot{\gamma}(t)$  as a function of the amplitude of the shear stress  $\sigma$ :

$$\begin{aligned} \dot{\gamma}(t) &= \frac{\gamma_c f_b}{\frac{G\gamma_c}{\sigma} - 1} = \dot{\gamma} \\ \Leftrightarrow \eta &= \frac{\sigma}{\dot{\gamma}} = \frac{\eta_0}{1 + \frac{\dot{\gamma}}{\gamma_c f_b}} = \frac{\sigma_f}{\gamma_c f_b + \dot{\gamma}}, \end{aligned} \quad (6)$$

with  $\eta_0 = G/f_b$  and  $\sigma_f = \eta_0 \gamma_c f_b = G\gamma_c$ .

As  $f_b$  is an increasing function of  $E_v$ , Eq. (6) shows that viscosity decreases when vibration energy increases (via the frequency  $f$  and/or the amplitude  $A$ ) or equivalently when granular temperature increases. This suggests that the sample should behave as a molecular condensed fluid [24]. In addition, Eq. (6) shows that the rheological behavior expected is viscous non-Newtonian, shear thinning. Furthermore, it reveals the existence of a Newtonian viscous regime at low shear rate ( $\eta \rightarrow \eta_0$  when  $\dot{\gamma} \rightarrow 0$ ) followed by a Coulombian

frictional regime at high shear rate ( $\sigma \rightarrow \sigma_f$  when  $\dot{\gamma} \rightarrow +\infty$ ). See Ref. [24] for a more extensive analysis. Before any experimental confrontation, the consistency of Eqs. (5) and (6) can be evaluated by examining extreme situations corresponding to two limiting cases:

(i) In the limit of small stresses, for  $\sigma(t) \ll G\gamma_c$  or equivalently for  $\dot{\gamma}(t)/\gamma_c \ll f_b$ , Eq. (4) becomes

$$\dot{\sigma}(t) + f_b \sigma(t) = G\dot{\gamma}(t). \quad (7)$$

Equation (7) is formally analogous to the Maxwell equation, usually written as  $\sigma(t) + \lambda(t)\dot{\sigma}(t) = \eta_0\dot{\gamma}(t)$  with  $\lambda = 1/f_b$  and  $\eta_0 = G/f_b$ . Consequently, all classical results of the *theory of linear viscoelasticity* associated with this model are, in principle, applicable to the case of vibrated granular media (cf § B.2). Equation (5) gives

$$\gamma(t) = \gamma_c \left[ \frac{f_b t}{\frac{G\gamma_c}{\sigma}} + \frac{\sigma}{G\gamma_c} \right] = \frac{\sigma}{G} (1 + f_b t) \quad \text{and} \quad \dot{\gamma}(t) = \frac{f_b \sigma}{G}, \quad (8)$$

with  $\ln(1 - \sigma/G\gamma_c) \cong -\sigma/G\gamma_c$ , since  $\sigma$  is much smaller than  $G\gamma_c$ .

By definition, in the limit of small stresses, the response to a step stress is used to determine the creep function  $J(t) = \gamma(t)/\sigma$ . Equation (8) shows that the expected response is such that  $J(t) = (1/G)(1 + f_b t)$ . Such a creep function is characteristic of a linear viscoelastic Maxwellian behavior, in agreement with Eq. (7). Furthermore, in full agreement with the properties of a Maxwellian fluid, Eq.(8) reveals that the granular system should behave as a Hookean solid at short times in such a way that  $\gamma(t) = \sigma/G = \gamma$  and as a Newtonian fluid at long times so that  $\dot{\gamma}(t) = \sigma/\eta_0$ , where  $\eta_0 = G/f_b$  is the Newtonian viscosity.

(ii) In the absence of vibrations ( $f_b = 0$ ) or for  $f_b \ll \dot{\gamma}(t)/\gamma_c$ , Eq. (4) becomes

$$\dot{\gamma}(t) = \gamma_c \frac{\dot{\sigma}(t)}{G\gamma_c - \sigma(t)}, \quad (9)$$

which, by integration with respect to  $\gamma(t)$  yields

$$\begin{aligned} \gamma(t) - \gamma(t_0) &= -\gamma_c \ln \left[ 1 - \frac{\sigma(t)}{G\gamma_c} \right] + \gamma_c \ln \left[ 1 - \frac{\sigma(t_0)}{G\gamma_c} \right] \\ &= -\gamma_c \ln \left[ \frac{1 - \frac{\sigma(t)}{G\gamma_c}}{1 - \frac{\sigma(t_0)}{G\gamma_c}} \right]. \end{aligned} \quad (10)$$

Equation (10) is only defined for  $\sigma(t) \leq G\gamma_c$ . In other words, Eq. (10) and the differential Eq. (4) from which it originated imply that there is a maximum stress  $\sigma_{\max} = G\gamma_c$  that cannot be exceeded, whatever the shear rate  $\dot{\gamma}$ . It can be shown [23,24] that this maximum stress can be identified to a frictional stress  $\sigma_f$  in agreement with Coulomb's law  $\sigma_f = \mu_f \sigma_n = \sigma_{\max}$ , where  $\mu_f$  is the coefficient of friction and  $\sigma_n$  the normal stress. Equation (5) can be written as

$$\gamma(t) = -\gamma_c \ln \left( 1 - \frac{\sigma}{G\gamma_c} \right) = \gamma. \quad (11)$$

When the frequency of reorganization  $f_b$  is zero, the granular medium is static and must behave like a solid. Equation (11) well captures such a feature and shows that the system behaves as an nonlinear elastic solid for which deformation increases "instantaneously" with the stress. In the limit of very low stresses, a first-order Taylor expansion of Eq. (11) gives  $\gamma(t) \cong \sigma/G$ , i.e., Hooke's equation that characterizes a linear elastic behavior, consistent with the Maxwellian limit of Eq. (4).

In the following, the consistency of the model was evaluated by fitting the equations derived from the integration of Eq. (4) to experimental data and by comparing the values obtained for the parameters  $G$ ,  $\eta_0$ ,  $\gamma_c$ , and  $\sigma_f$  via the different tests. Figure 4 displays for a vibrated sample, the evolution with time of  $\gamma(t)$  for applied stresses of 1, 3, 10, and 30 Pa. A linear deformation is observed in agreement with the prediction of Eqs. (5) and (8). As an illustration, for  $\sigma = 10$  Pa, the fit of Eq. (8) yields  $\sigma/\eta_0 = 0.0181 \text{ s}^{-1}$  and  $\eta_0 = 552 \text{ Pa s}$ , where  $\eta_0 = G/f_b$ .

Figure 5 displays for nonvibrated samples subjected to stress steps of 1, 3, 10, 20, 30, 40, and 50 Pa, the evolution

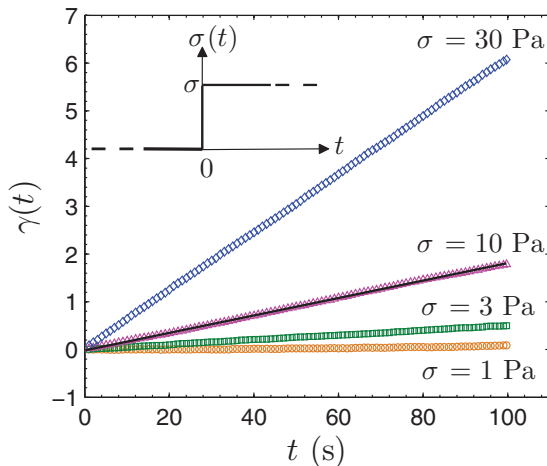


FIG. 4. (Color online) Temporal evolution of the strain  $\gamma(t)$  for stress step of 1, 3, 10, and 30 Pa, under vibrations ( $f = 50 \text{ Hz}$  and  $E_v = 164 \mu\text{J}$ ). The solid line materializes the fit of Eq. (8) to the experimental points.

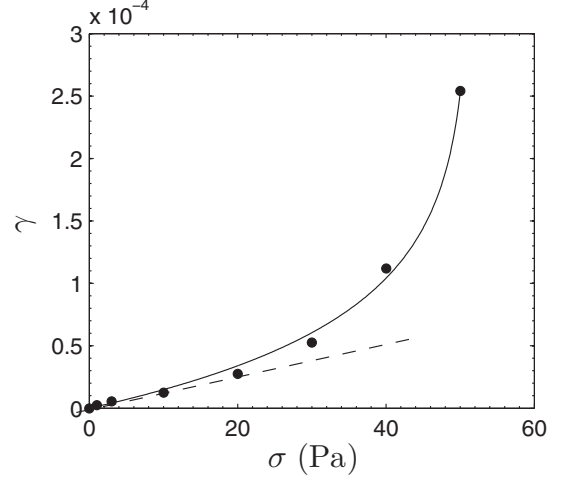


FIG. 5. Evolution of the deformation ( $\gamma$ ) as a function of the stress ( $\sigma$ ), in the absence of vibration ( $f = 0 \text{ Hz}$  and  $E_v = 0 \mu\text{J}$ ). The solid line materializes the fit of Eq. (11) to the experimental points. The dotted line shows the Hookean limit of the behavior of the sample at low stresses.

of the average strain value ( $\gamma$ ) as a function of the imposed stress ( $\sigma$ ). The solid line corresponds to the fit of Eq. (11) to the experimental data. The fit yields  $\gamma_c = 6.88 \times 10^{-5}$  and  $G\gamma_c = 51.3 \text{ Pa} \Rightarrow G = 7.45 \times 10^5 \text{ Pa}$ . The agreement between experimental data and the fitted curve related to Eq. (11) reveals that the model provides an excellent description of the static behavior of the samples up to stress values around 50 Pa. For higher values, stick-slip instabilities perturbing the rheometer loop control start occurring resulting in measurement fluctuations. But when the stress rises above 148 Pa, a steady, frictional flow appears. Since the shear rate is now constant, an effective viscosity can now be calculated, and this viscosity is shown in Fig 6. It is worth noting that the

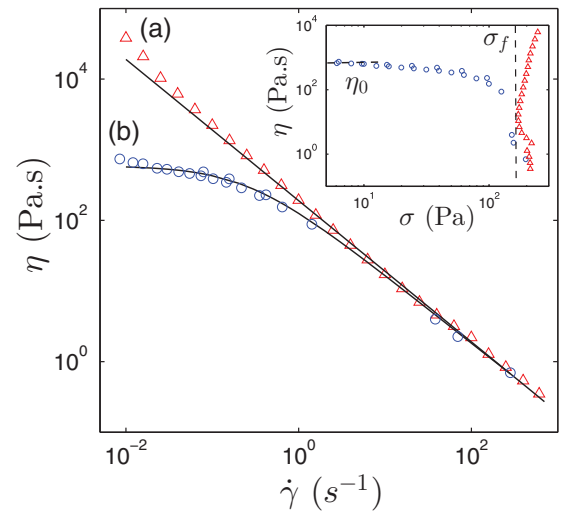


FIG. 6. (Color online) Evolution of the viscosity ( $\eta$ ) in steady-state regime as a function of the shear rate ( $\dot{\gamma}$ ): (a) without vibrations ( $f = 0 \text{ Hz}$  and  $E_v = 0 \mu\text{J}$ ), (b) under vibration ( $f = 50 \text{ Hz}$  and  $E_v = 164 \mu\text{J}$ ). The solid lines materialize the fit of Eq. (6) to the experimental points. Inset, the same data were plotted against the shear stress.

experiment of Fig. 5 corresponds to a static regime, until the frictional stress is reached leading to the frictional flow regime observed in Fig. 6(a). Stick-slip instabilities mark the transition between these two regimes. It also appears that in the low stress limit ( $\sigma < 20$  Pa), a Hookean behavior is obtained in agreement with Eq. (11).

As previously mentioned, step stress experiments can be used to extract the evolution of viscosity  $\eta = \sigma/\dot{\gamma}$ , as a function of shear rate. Figure 6 displays the results of such a measurement, with and without vibrations, in steady-state flow regime, contrary to the previous experiment. In this figure the solid line corresponds to the fit of Eq. (6) to the experimental data. The fit of Eq. (6) to curve (b) yields to  $\eta_0 = G/f_b = 592$  Pa s and  $\dot{\gamma}_c = \gamma_c f_b = 0.25$  s $^{-1}$   $\Rightarrow \sigma_f = \eta_0 \dot{\gamma}_c = G\gamma_c = 148$  Pa. This value of  $\sigma_f$  matches the value found by fitting Eq. (6) to curve (a) since curves (a) and (b) collapse beyond  $\dot{\gamma} = 10$  s $^{-1}$ . The value of  $\eta_0$  thus determined (592 Pa s) is, considering experimental errors, very close to that determined from creep tests (552 Pa s). This figure is also evidence of the existence of a Newtonian regime at low stress and of a nonlinear Coulombian one at high stress, features that agree with Eq. (6). The difference between the values of  $\sigma_f$  extracted from Fig. 5 (51.3 Pa) and from Fig. 6 (148 Pa) comes from the fact that both experiments have been performed in two different regimes: a flow regime and a static one. It is worth noting that it is experimentally challenging to extract  $\sigma_f$ , which is a dynamical quantity, from a static experiment via the relation  $\sigma_f = G\gamma_c$ . Additionally, the divergence of the curve in the vicinity of  $\sigma_f$  hinders a precise numerical determination of its value. Despite these difficulties, both values remain of the same order of magnitude.

## 2. Response to a sinusoidal stress

In the case of a sinusoidal stress defined as  $\sigma(t) = \sigma_o \cos(\omega t)$  and  $\dot{\sigma}(t) = -\omega \sigma_o \sin(\omega t)$  (Fig. 7), with  $\sigma_o$  the oscillation amplitude and  $\omega$  the pulsation, useful information can be obtained without a full integration of Eq. (4). Letting  $\tan \delta = f_b/\omega$ , Eq (4) yields

$$\begin{aligned} \dot{\gamma}(t) &= \gamma_c \frac{\dot{\sigma}(t) + f_b \sigma(t)}{G\gamma_c - \sigma(t)} = -\gamma_c \frac{\omega \sin(\omega t) - f_b \cos(\omega t)}{\frac{G\gamma_c}{\sigma_o} - \cos(\omega t)} \\ &= -\gamma_c \frac{(\omega^2 + f_b^2)^{1/2} \sin(\omega t - \delta)}{\frac{G\gamma_c}{\sigma_o} - \cos(\omega t)}. \end{aligned} \quad (12)$$

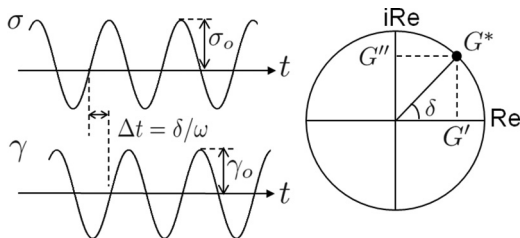


FIG. 7. Measurement principle in oscillatory regime (mechanical spectroscopy).

In the limit of small stresses ( $\sigma_o \ll G\gamma_c$ ) and under vibrations, Eq. (12) yields

$$\begin{aligned} \dot{\gamma}(t) &= -\frac{\sigma_o}{G} (\omega^2 + f_b^2)^{1/2} \sin(\omega t - \delta) \\ \Rightarrow \gamma(t) &= \frac{\sigma_o}{\omega G} (\omega^2 + f_b^2)^{1/2} \cos(\omega t - \delta). \end{aligned} \quad (13)$$

Equation (13) could have been obtained directly by solving Maxwell's equation,  $\delta$  being the phase angle between  $\sigma(t)$  and  $\gamma(t)$  (Fig. 7) and  $\tan \delta = f_b/\omega = 1/(\lambda\omega)$ , where  $\lambda = 1/f_b$ . According to this result, the system should behave as a linear viscoelastic one as long as the denominator of Eq. (12) does not diverge, i.e., for  $\sigma_o$  not too close to  $G\gamma_c$ , i.e., as long as the system does not enter the frictional regime. Letting  $\sigma(t) = \text{Re}\{\tilde{\sigma}(t) = \sigma_o e^{i\omega t}\}$  and  $\gamma(t) = \text{Re}\{\tilde{\gamma}(t) = \gamma_o e^{i(\omega t - \delta)}\}$ , the resolution of the complex form of Eq. (7) gives, classically,

$$\begin{aligned} G^*(\omega) &= \frac{\tilde{\sigma}(t)}{\tilde{\gamma}(t)} = \frac{\sigma_o e^{i\delta}}{\gamma_o} \\ &= \frac{G\omega^2 \lambda^2}{1 + \omega^2 \lambda^2} + i \frac{G\omega \lambda}{1 + \omega^2 \lambda^2} = G' + iG'', \end{aligned} \quad (14)$$

with

$$G' = G \frac{\omega^2 \lambda^2}{1 + \omega^2 \lambda^2} \text{ and } G'' = G \frac{\omega \lambda}{1 + \omega^2 \lambda^2}. \quad (15)$$

$G' = \frac{\sigma_o}{\gamma_o} \cos \delta$  being the elastic modulus and  $G'' = \frac{\sigma_o}{\gamma_o} \sin \delta$  the viscous modulus. Noting that  $f_b \in [0; +\infty[$  and  $\omega \in [0; +\infty[$   $\Rightarrow \tan \delta \in [0; +\infty[$ , one has  $\delta \in [0; \pi/2]$ , in agreement with Hookean ( $\delta = 0$ ) and Newtonian ( $\delta = \pi/2$ ) limits.

To test the model, we first carried out a stress sweep test, in which the stress amplitude  $\sigma_o$  was varied at a fixed frequency ( $\omega = 1$  rad s $^{-1}$ ), under vibrations ( $f = 50$  Hz and  $E_v = 164$   $\mu$ J). Such an experiment provides values for  $\sigma_o$ ,  $\gamma_o$  and the phase angle  $\delta$  (Fig. 7) that can be directly compared to the predictions of Eq. (12). As in the experimental conditions used (Fig. 4),  $75^\circ \leq \delta \leq 90^\circ$ , then  $\sin(\omega t - \delta) \cong -\cos(\omega t)$ . Consequently, Eq. (12) can be written as

$$\dot{\gamma}_o = \max\{\dot{\gamma}(t)\} \cong \gamma_c \frac{(\omega^2 + f_b^2)^{1/2}}{\frac{G\gamma_c}{\sigma_o} - 1}. \quad (16)$$

Figure 8 displays the evolution of the maximum amplitude of the strain rate  $\dot{\gamma}_o = \omega \gamma_o$  as a function of  $\sigma_o$ . As shown by the solid line plotted in Fig. 8, Eq. (16) accurately fits the experimental data and yields  $\gamma_c (\omega^2 + f_b^2)^{1/2} = 0.357$  s $^{-1}$  and  $G\gamma_c = \sigma_f = 201$  Pa. This latter value for the frictional stress is close to the value previously obtained  $\sigma_f = 148$  Pa in steady-state regime (Fig. 6). Furthermore, low-stress data exhibit a linear dependence on  $\sigma_o$ , whereas for higher stress a clear divergence is observed in agreement with Eq. (16). Figure 8 shows that the linear viscoelastic domain appears to extend up to a critical shear rate value  $\dot{\gamma}_c \approx 0.1$  s $^{-1}$  that corresponds to a critical strain  $\gamma_c = \dot{\gamma}_c/\omega \approx 0.1$ , as  $\omega = 1$  rad s $^{-1}$  in the corresponding experiment. It leads to  $G = \sigma_f/\gamma_c \approx 2000$  Pa.

Figure 9 corresponds to a frequency sweep test carried out on the same sample under the same vibration energy. In this experiment, the values of  $G'$  and  $G''$  are measured for various frequencies  $\omega$  at a fixed amplitude stress  $\sigma_o$ , the value of which

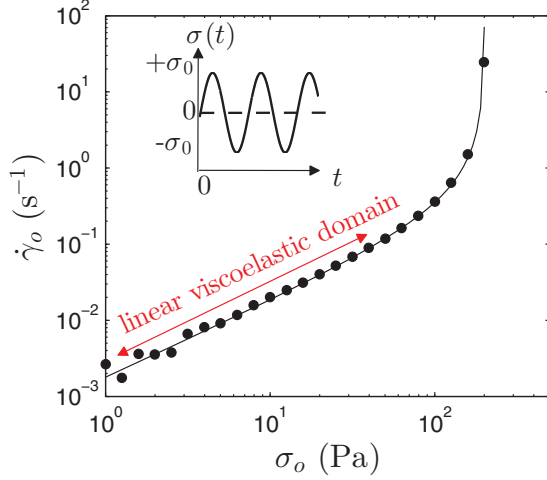


FIG. 8. (Color online) Evolution of the maximum amplitude of the strain rate ( $\dot{\gamma}_0$ ) as a function of the maximum amplitude of the stress ( $\sigma_0$ ) for  $\omega = 1 \text{ rad s}^{-1}$ , under vibrations ( $f = 50 \text{ Hz}$  and  $E_v = 164 \mu\text{J}$ ). The solid line materializes the fit of Eq. (16) to the experimental points.

(10 Pa) was chosen in the linear viscoelastic domain. The solid lines in Fig. 9 correspond to a fit according to Eq. (15) that yields  $G = 1792 \text{ Pa}$  and  $\lambda = 0.31 \text{ s}$ . It must be pointed out that the value of  $G$ , thus determined, is close to that derived from stress sweep test ( $\approx 2000 \text{ Pa}$ ). Furthermore, these values allow determining  $f_b = 1/\lambda = 3.23 \text{ s}^{-1}$  and  $\eta_0 = G/f_b = 555 \text{ Pa s}$ . The fact that this latter value is very close to that determined previously from creep experiments illustrates the robustness of the model we propose.

Closer examination of Fig. 9 reveals additional trends. It appears that Eq. (15) captures well the mechanical properties of the system at low  $\omega$  values, i.e., when the viscous behavior dominates ( $G'' > G'$ ). In this region,  $G'$  evolves as  $\omega^2$  and  $G''$  as  $\omega$  in agreement with a Maxwellian behavior. In contrast, data

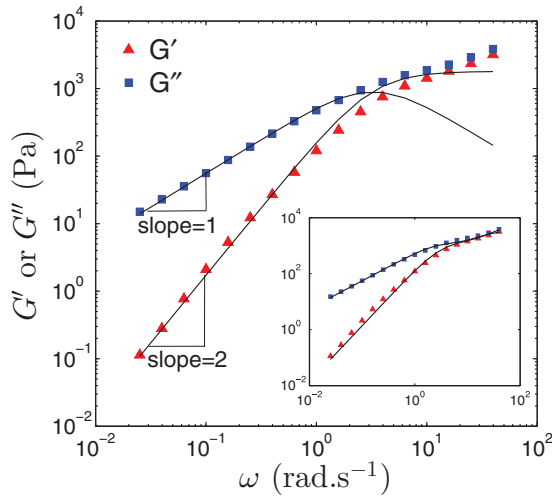


FIG. 9. (Color online) Evolution of the elastic modulus ( $G'$ ) and the viscous modulus ( $G''$ ) as a function of pulsation ( $\omega$ ) for a maximum stress amplitude  $\sigma_0 = 10 \text{ Pa}$ , under vibrations ( $f = 50 \text{ Hz}$  and  $E_v = 164 \mu\text{J}$ ). Solid lines materialize the fit of Eqs. (15) and (17) (inset) to the experimental points.

at higher  $\omega$  values, past the  $G'/G''$  crossover, are not properly described by Eq. (15). Such a discrepancy between model and experiment can be assigned to the fact that our model only considers one mechanism for relaxation processes, whereas, in fact, as in molecular media, two mechanisms should be taken into account:  $\alpha$ -relaxation and  $\beta$ -relaxation. The  $\alpha$ -process corresponds to the diffusion of grains out of the cage formed by their nearest neighbors. Such a process allows sample flow. It dominates the viscous rheological behavior at low  $\omega$  values (Fig. 9). The  $\beta$ -process corresponds to the diffusion of grains within the cage formed by their nearest neighbors. The characteristic time  $t_\beta$  corresponding to this latter process is obviously shorter than that of the  $\alpha$ -relaxation ( $t_\alpha$ ) and it may then start playing a role for high pulsations. In order to take into account these two processes, it is possible to introduce two relaxation times,  $\lambda_1$  and  $\lambda_2$ , and two weighing factors,  $G_1$  and  $G_2$ , in the Maxwell model, such as

$$G' = G_1 \frac{\omega^2 \lambda_1^2}{1 + \omega^2 \lambda_1^2} + G_2 \frac{\omega^2 \lambda_2^2}{1 + \omega^2 \lambda_2^2} \quad (17)$$

$$G'' = G_1 \frac{\omega \lambda_1}{1 + \omega^2 \lambda_1^2} + G_2 \frac{\omega \lambda_2}{1 + \omega^2 \lambda_2^2}.$$

Letting  $\lambda_1 = t_\alpha$ ,  $\lambda_2 = t_\beta$  and remembering that  $f = 50 \text{ Hz}$  and that  $f_b$  was estimated to  $3.23 \text{ s}^{-1}$  in the low  $\omega$  region yields  $\lambda_1 = t_\alpha = f_b^{-1} = 0.31 \text{ s}$  and  $\lambda_2 = t_\beta = f^{-1} = 0.02 \text{ s}$ . Using such values of  $\lambda_1$  and  $\lambda_2$  in Eq. (17) leads to  $G_1 = 1400 \text{ Pa}$  and  $G_2 = 6000 \text{ Pa}$ . As shown in Fig. 9, considering two relaxation processes significantly improves the agreement between model and experiments. Considering two characteristic times was, however, not required for the modeling of creep experiments. This is likely due to the fact that creep tests provide accurate rheological information for long times only. Due to inertial effects in the rheometer and to the times associated to signal acquisition, creep tests cannot be used reliably to investigate processes with short characteristic times.

In order to provide an overview of the results of the different experiments, Table I displays the numerical values of the model parameters determined by adjustment to experimental points, without vibrations and with vibrations for a vibration energy  $E_v = 164 \mu\text{J}$ . The dependence of the model parameters, i.e., the shear modulus ( $G$ ), the critical strain ( $\gamma_c$ ), and the Brownian frequency reorganization of the grains ( $f_b$ ) with the vibration energy ( $E_v$ ) is shown in Appendix A.

#### IV. CONCLUSIONS AND PERSPECTIVES

On the basis of simple experimental procedures, and using a few reasonable assumptions, we have been able to derive an elementary differential equation that is able to capture various rheological behaviors (in transient or steady-state regimes and in the presence and absence of vibrations) using three independent parameters only ( $G$ ,  $\gamma_c$ ,  $f_b$ ). The exact solution of the model takes the form of a constitutive equation relating stress to strain from which all rheological properties can be derived. The solution predicts viscous (Newtonian) and frictional (Coulombian) regimes, as well as elastic linear (Hookean) and nonlinear behaviors that are qualitatively and quantitatively in agreement with experiments. Within experimental errors, parameters values are independent of the type of test used (linear, nonlinear, permanent, transient, or oscillatory).

TABLE I. Numerical values of the model parameters, with vibrations (up) and without vibrations (down). Numbers in brackets have been obtained on the basis of the value  $\gamma_c = 0.1$ , determined in oscillatory regime.

$f = 50$ Hz $E_v = 164 \mu\text{J}$	$G$ (Pa)	$f_b$ ( $\text{s}^{-1}$ )	$\gamma_c$ (-)	$\eta_0 = G/f_b$ (Pa s)	$\sigma_f = G\gamma_c$ (Pa)	$\dot{\gamma}_c = \gamma_c f_b$ ( $\text{s}^{-1}$ )
Creep tests (Figs. 4 * and 6 <sup>‡</sup> )	(1480)	(2.50)	(0.1)	552*–592 <sup>‡</sup>	148	0.25
Oscillatory tests (Figs. 8 <sup>¶</sup> and 9 <sup>†</sup> )	2000 <sup>¶</sup> –1792 <sup>†</sup>	3.23	0.1	555	179 <sup>¶</sup> –201 <sup>†</sup>	0.323
$f = 0$ Hz $E_v = 0 \mu\text{J}$	$G$ (Pa)	$f_b$ ( $\text{s}^{-1}$ )	$\gamma_c$ (-)	$\eta_0 = G/f_b$ (Pa s)	$\sigma_f = G\gamma_c$ (Pa)	$\dot{\gamma}_c = \gamma_c f_b$ ( $\text{s}^{-1}$ )
Creep tests (Figs. 5* and 6 <sup>‡</sup> )	$7.45 \times 10^5$	0	$6.88 \times 10^{-5}$	$\infty$	51.3*–148 <sup>‡</sup>	0

These results strongly suggest that the rheological response of vibrated granular media, subjected to nonstationary stress, can be described by a simple “two-states model” related to the inherent bimodal behavior of chain forces [13–16]. They also tend to show that the dynamics of vibrated granular materials can be viewed as a kinetic process based on transitions from a “strong state,” which ensures momentum transport, to a flowing state. Hopping rates then depend on the intensity of both shear and vibration. We have shown that the high-frequency (short-time) behavior could be described by introducing two relaxation times in the Maxwell model related to the  $\alpha$  and  $\beta$  relaxation processes commonly observed in granular matter [48,49].

A particularly noteworthy aspect of the present study is related to the fact that the model is able to capture both flow experiments and mechanical spectroscopy ones. This is generally not achieved in the rheological modeling of molecular or colloidal systems. Most common rheological models, such as SGR or STZ, fail to include local flow and plastic events in a coarse-grained variable in a continuous field. Another loophole in most existing models lies in the introduction of an effective temperature, the meaning of which is often rather obscure. This effective temperature, associated to the noise level in the medium, controls the degrees of freedom whose changes cause the system to move from one energy minimum to another in a continuous energy landscape. Such difficulty is ironed out in the present paper for granular matter subjected to vibrations. In this case, granular reorganization is controlled by applied vibrations at low stress that correspond to an external temperature as discussed by D’Anna *et al.* [33]. Our model describes the macroscopic behavior of granular matter regardless of nonlocal flows effects mentioned in the literature [50–52]. The main reason is that a potential localization of the flow also leads to a frictional behavior, which is captured by the model. Moreover, our results suggest that these nonlocal flow effects vanish in the regime controlled by vibrations where the flow remains Newtonian.

In the near future, it would be of interest to try to extend this model to saturated granular suspensions. In such systems, understanding the viscoelastic behavior will require taking into account, in addition to vibrations, effects related to the viscosity of the interstitial fluid. We recently evidenced coupling between these two parameters [53] and it would be particularly relevant to see if the viscosity of the suspending fluid could be introduced in a kinetic equation [Eq. (3)],

to derive for granular suspensions a similar self-consistent approach as that derived for dry granular systems.

#### APPENDIX A: EVOLUTION OF THE MODEL PARAMETERS ( $G$ , $\gamma_c$ , $f_b$ ) AS A FUNCTION OF THE VIBRATION ENERGY $E_v$

Creep tests and mechanical spectroscopy experiments were also carried out for different values of vibration energies, ranging from 0 to 742  $\mu\text{J}$ . For each applied energy, the adjustment of the model to the experimental data allows us to obtain  $G$ ,  $\gamma_c$ , and  $f_b$ . Figure 10 shows the evolution of these parameters as a function of the vibration energy.

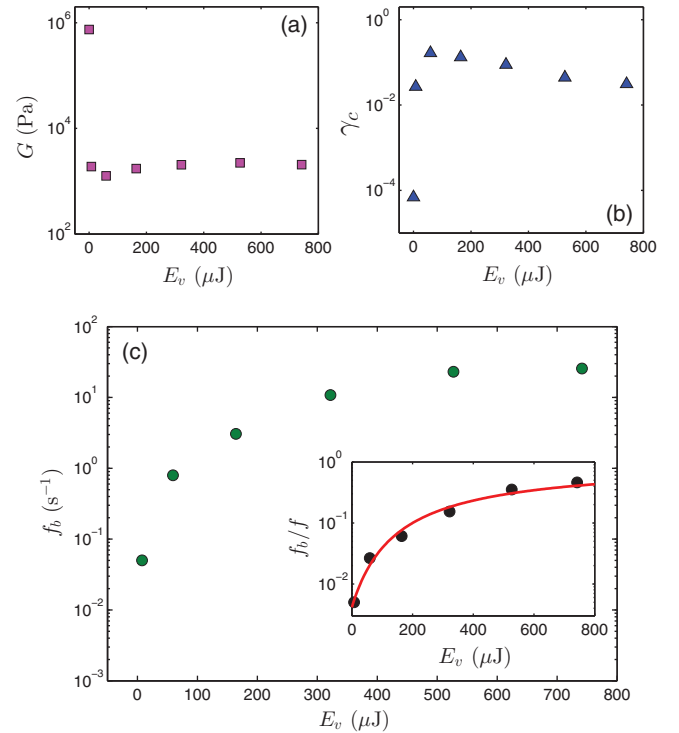


FIG. 10. (Color online) Evolution of the model parameters, i.e., (a) the shear modulus ( $G$ ), (b) the critical strain, and (c) the Brownian reorganization frequency of the grains ( $f_b$ ), as a function of the vibration energy ( $E_v$ ). In the inset, symbols represent the evolution of  $f_b/f$ , with  $f$  the vibration frequency, as a function of  $E_v$ , and the solid line represents the fit of Eq. (A1) to the experimental points.

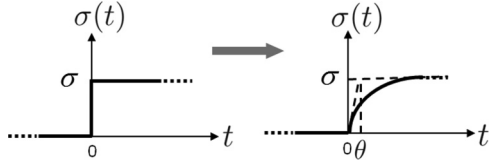


FIG. 11. Substitution of a stress step by an exponential function.

Under vibrations ( $E_v > 0 \mu\text{J}$ ), the shear modulus  $G$  [Fig. 10(a)] and the critical strain  $\gamma_c$  [Fig. 1(b)] are constant and are nearby equal to 2000 and 0.1 Pa, respectively. The application of vibrations, even of low energy, change dramatically the values of  $G$  and  $\gamma_c$ . Indeed,  $G$  falls from  $7.45 \times 10^5$  Pa without vibrations to around 2000 Pa with vibrations and  $\gamma_c$  increases from  $6.88 \times 10^{-5}$  Pa without vibrations to around 0.1 Pa with vibrations. This effect has already been highlighted by Marchal *et al.* [24], by showing that any finite amplitude vibration suppressed the yield stress and led to a viscosity plateau.

Contrary to  $G$  and  $\gamma_c$ , the reorganization frequency  $f_b$  is not constant under vibrations ( $E_v > 0 \mu\text{J}$ ) and increases with  $E_v$ , as mentioned in Sec. III A and as shown by Marchal *et al.* [24]. Knowing that  $f_b = G/\eta_0$ , the combination of Eqs. (11) and (31) presented in Ref. [24] leads to

$$f_b = f \exp \left[ \frac{-\varepsilon_2}{E_v + \varepsilon_3 \left( \frac{\phi_m - \phi_{rcp}}{\phi_m} \right)} \right], \quad (\text{A1})$$

where  $\varepsilon_2$  and  $\varepsilon_3$  are constants,  $f$  is the vibration frequency,  $\phi_m$  is the maximum packing fraction ( $=0.74$ ), and  $\phi_{rcp}$  is the random close packing fraction ( $=0.62$ ).

In the inset of Fig. 10(c), the experimental data are correctly fitted to Eq. (A1) with  $\varepsilon_2 = 794 \mu\text{J}$  and  $\varepsilon_3 = 893 \mu\text{J}$ , which proves the robustness of the model presented in Ref. [24].

## APPENDIX B: DERIVATION OF EQUATION (5)

In the case of a stress step defined as  $\sigma(t) = 0$  for  $t < 0$  and  $\sigma(t) = \sigma$  for  $t > 0$  (Fig. 11), the choice of the initial value  $\sigma(t=0)$  is arbitrary and the derivative  $\dot{\sigma}(t=0)$  is discontinuous. In linear situations, these signals are easily treated by Laplace transform and integration of Eq.(4), which reduces to Maxwell equation, is no problem. In contrast, the incorporation of the term  $\dot{\gamma}(t)/\gamma_c$  introduces nonlinearity, which invalidates the application of these methods.

In this case, the differential Eq. (4) can be integrated using functions more regular, continuous, and unambiguously

defined at  $t = 0$  tending toward a step when a temporal parameter  $\theta$  tends to zero. In the present situation, the stress step can be replaced by an exponential function such as  $\sigma(t) = 0$  for  $t \leq 0$  and  $\sigma(t) = \sigma(1 - e^{-t/\theta})$  for  $t \geq 0$ . By incorporating the exponential function  $\sigma(t) = \sigma(1 - e^{-t/\theta})$  in Eq. (4) one obtains

$$\begin{aligned} \dot{\gamma}(t) &= \gamma_c \frac{\dot{\sigma}(t) + f_b \sigma(t)}{G\gamma_c - \sigma(t)} = \gamma_c \frac{\frac{\sigma}{\theta} e^{-t/\theta} + f_b \sigma(1 - e^{-t/\theta})}{G\gamma_c - \sigma(1 - e^{-t/\theta})} \\ &= \gamma_c \frac{\left(\frac{\sigma}{\theta} - f_b \sigma\right) e^{-t/\theta} + f_b \sigma}{\left(G\gamma_c - \sigma\right) + \sigma e^{-t/\theta}} \\ &= \gamma_c \frac{\left(\frac{1}{\theta} - f_b\right) e^{-t/\theta}}{\left(\frac{G\gamma_c}{\sigma} - 1\right) + e^{-t/\theta}} + \gamma_c \frac{f_b}{\left(\frac{G\gamma_c}{\sigma} - 1\right) + e^{-t/\theta}}. \quad (\text{B1}) \end{aligned}$$

Noting that  $\int \frac{e^{cx}}{a+be^{cx}} dx = \frac{1}{bc} \ln(a + be^{cx})$  and  $\int \frac{dx}{a+be^{cx}} = \frac{x}{a} - \frac{1}{ac} \ln(a + be^{cx})$ , it follows that

$$\begin{aligned} \gamma(t) &= \gamma_c \frac{f_b t}{\left(\frac{G\gamma_c}{\sigma} - 1\right)} - \theta \ln \left[ \frac{1}{\gamma_c} \left( \frac{G\gamma_c}{\sigma} - 1 \right) + \frac{1}{\gamma_c} e^{-t/\theta} \right] \\ &\quad \times \left[ \gamma_c \left( \frac{1}{\theta} - f_b \right) - \gamma_c \frac{f_b}{\left(\frac{G\gamma_c}{\sigma} - 1\right)} \right] + \text{cte} \\ &= \gamma_c \frac{f_b t}{\left(\frac{G\gamma_c}{\sigma} - 1\right)} - \ln \left[ \frac{1}{\gamma_c} \left( \frac{G\gamma_c}{\sigma} - 1 \right) + \frac{1}{\gamma_c} e^{-t/\theta} \right] \\ &\quad \times \left[ \gamma_c (1 - \theta f_b) - \gamma_c \frac{\theta f_b}{\left(\frac{G\gamma_c}{\sigma} - 1\right)} \right] + \text{cte}. \quad (\text{B2}) \end{aligned}$$

Letting  $\gamma(0) = 0$ , one obtains

$$\text{cte} = \ln \frac{G}{\sigma} \left[ \gamma_c (1 - \theta f_b) - \gamma_c \frac{\theta f_b}{\left(\frac{G\gamma_c}{\sigma} - 1\right)} \right]. \quad (\text{B3})$$

Differentiating  $\gamma(t)$  before letting  $\theta$  tending toward 0, it can be verified that Eq. (B2) is indeed a solution of Eq. (4) with  $\sigma(t) = \sigma(1 - e^{-t/\theta})$ . When  $\theta \rightarrow 0$ ,  $\sigma(t)$  tends toward a step function such as  $\sigma(t) = \sigma$  for  $t > 0$ , as a result  $\text{cte} \rightarrow \gamma_c \ln(G/\sigma)$  and

$$\begin{aligned} \gamma(t) &= \gamma_c \frac{f_b t}{\left(\frac{G\gamma_c}{\sigma} - 1\right)} - \gamma_c \ln \frac{1}{\gamma_c} \left( \frac{G\gamma_c}{\sigma} - 1 \right) + \gamma_c \ln \left( \frac{G}{\sigma} \right) \\ &= \gamma_c \left[ \frac{f_b t}{\frac{G\gamma_c}{\sigma} - 1} - \ln \left( 1 - \frac{\sigma}{G\gamma_c} \right) \right] + \text{cte}. \quad (\text{B4}) \end{aligned}$$

[1] P. Sollich, F. Lequeux, P. Hebraud, and M. E. Cates, *Phys. Rev. Lett.* **78**, 2020 (1997).  
[2] P. Sollich, *Phys. Rev. E* **58**, 738 (1998).  
[3] J.M. Brader, M. Siebenburger, M. Ballauff, K. Reinheimer, M. Wilhelm, S. J. Frey, F. Weysser, and M. Fuchs, *Phys. Rev. E* **82**, 061401 (2010).  
[4] E. Bouchbinder and J. S. Langer, *Phys. Rev. E* **83**, 061503 (2011).

[5] R. P. Behringer, D. Bi, B. Chakraborty, S. Henkes, and R. R. Hartley, *Phys. Rev. Lett.* **101**, 268301 (2008).  
[6] G. Midi, *Eur. Phys. J. E* **14**, 341 (2004).  
[7] Y. Forterre and O. Pouliquen, *Annu. Rev. Fluid. Mech.* **40**, 1 (2008).  
[8] K. A. Reddy, Y. Forterre, and O. Pouliquen, *Phys. Rev. Lett.* **106**, 108301 (2011).

- [9] C. H. Liu, S. R. Nagel, D. A. Schecter, S. N. Coppersmith, S. Majumdar, O. Narayan, and T. A. Witten, *Science* **269**, 5223 (1995).
- [10] J. H. Snoeijer, T. J. H. Vlugt, M. vanHecke, and W. vanSaarloos, *Phys. Rev. Lett.* **92**, 054302 (2004).
- [11] S. Ostojic, E. Somfai, and B. Nienhuis, *Nature (London)* **439**, 828 (2006).
- [12] L. Staron and F. Radjai, *Phys. Rev. E* **72**, 041308 (2005).
- [13] S. Deboeuf, O. Dauchot, L. Staron, A. Mangeney, and J. P. Vilotte, *Phys. Rev. E* **72**, 051305 (2005).
- [14] V. Y. Zaitsev, P. Richard, R. Delannay, V. Tournat, and V. E. Gusev, *Europhys. Lett.* **83**, 64003 (2008).
- [15] S. K. de Richter, V. Y. Zaitsev, P. Richard, R. Delannay, G. L. Caer, and V. Tournat, *J. Stat. Mech.* (2010) P11023.
- [16] F. Radjai, D. E. Wolf, M. Jean, and J. J. Moreau, *Phys. Rev. Lett.* **80**, 61 (1998).
- [17] G. H. Darwin, *Minutes of Proceedings of Institute of Civil Engineering* **71**, 350 (1883).
- [18] P. G. de Gennes, *Physica A* **261**, 267 (1998).
- [19] L. Vanel, D. W. Howell, D. Clark, R. P. Behringer, and E. Clement, *Phys. Rev. E* **60**, R5040 (1999).
- [20] P. Marchal, A. Barois-Cazenave, and L. Choplin, *Les Cahiers de Rhéologie* **16**, 143 (1999).
- [21] P. Marchal, Ph.D. thesis, Institut Polytechnique de Lorraine, Nancy, France, 2002.
- [22] P. Marchal, N. Smirani, and L. Choplin, in *39<sup>ème</sup> Colloque Annuel du Groupe Français de Rhéologie* (Mulhouse, France, 2004).
- [23] P. Marchal, L. Choplin, and N. Smirani, *Rhéologie des milieux granulaires denses vibrés*, Vol. 14 (Les Cahiers de Formulation, Formulation des solides divisés, EDP Sciences, 2009), pp. 139–151.
- [24] P. Marchal, L. Choplin, and N. Smirani, *J. Rheol.* **53**, 1 (2009).
- [25] E. Clement and J. Rajchenbach, *Europhys. Lett.* **16**, 133 (1991).
- [26] G. D’Anna and G. Gremaud, *Nature (London)* **413**, 407 (2001).
- [27] G. D’Anna and G. Gremaud, *Phys. Rev. Lett.* **87**, 254302 (2001).
- [28] P. Philippe and D. Bideau, *Europhys. Lett.* **60**, 677 (2002).
- [29] J. B. Knight, C. G. Fandrich, C. N. Lau, H. M. Jaeger, and S. R. Nagel, *Phys. Rev. E* **51**, 3957 (1995).
- [30] S. K. de Richter, G. L. Caer, and R. Delannay, *J. Stat. Mech.* (2012) P04013.
- [31] S. K. de Richter, G. L. Caer, and R. Delannay, *EPL* **85**, 58004 (2009).
- [32] J. A. Dijksman, G. H. Wortel, L. T. H. vanDellen, O. Dauchot, and M. vanHecke, *Phys. Rev. Lett.* **107**, 108303 (2011).
- [33] G. D’Anna, P. Mayor, A. Barrat, V. Loreto, and F. Nori, *Nature (London)* **424**, 909 (2003).
- [34] G. D’Anna, P. Mayor, G. Gremaud, A. Barrat, and V. Loreto, *Europhys. Lett.* **61**, 60 (2003).
- [35] G. D’Anna and P. Mayor, *Physica A* **325**, 267 (2003).
- [36] P. Marchal, L. Choplin, and N. Smirani, US Patent 6 971, 262 (2005).
- [37] S. F. Edwards and R. B. S. Oakeshott, *Physica A* **157**, 1080 (1989).
- [38] D. S. Dean and A. Lefevre, *Phys. Rev. Lett.* **90**, 198301 (2003).
- [39] T. Aste and T. DiMatteo, *Phys. Rev. E* **77**, 021309 (2008).
- [40] S. McNamara, P. Richard, S. K. deRichter, G. LeCaer, and R. Delannay, *Phys. Rev. E* **80**, 031301 (2009).
- [41] J. Duran, *Sands, Powders, and Grains: An Introduction to the Physics of Granular Materials*, Vol. 216 (Springer, Berlin, 2000), p. 293.
- [42] O. Reynolds, *Philos. Mag. Soc.* **20**, 469 (1885).
- [43] O. Reynolds, Proceedings of the Royal Institution of Great Britain, Read, February 12, 1886 (unpublished).
- [44] P. de Gennes, *J. Colloid Interface Sci.* **226**, 1 (2000).
- [45] Markovian stationary processes.
- [46] Molecular chaos assumption of Boltzmann.
- [47] P. Coussot, *Rhéophysique des pâtes et des suspensions* (EDP Sciences/CNRS Editions, Les Ulis, 1999).
- [48] G. Marty and O. Dauchot, *Phys. Rev. Lett.* **94**, 015701 (2005).
- [49] P. M. Reis, R. A. Ingale, and M. D. Shattuck, *Phys. Rev. Lett.* **98**, 188301 (2007).
- [50] D. M. Mueth, G. F. Debregeas, G. S. Karczmar, P. Eng, S. R. Nagel, and H. M. Jaeger, *Nature* **406**, 385 (2000).
- [51] A. Fall, F. Bertrand, G. Ovarlez, and D. Bonn, *Phys. Rev. Lett.* **103**, 178301 (2009).
- [52] K. Kamrin and G. Koval, *Phys. Rev. Lett.* **108**, 178301 (2012).
- [53] C. Hanotin, S. Kiesgen de Richter, P. Marchal, L. J. Michot, and C. Baravian, *Phys. Rev. Lett.* **108**, 198301 (2012).